Research Article

A Novel Low-Profile 5G MIMO Antenna for Vehicular Communication

Malathi Kanagasabai [ID],[1] Shanmathi Shanmuganathan [ID],[1] M. Gulam Nabi Alsath [ID],[2] and Sandeep Kumar Palaniswamy [ID][3]

[1]*Department of Electronics and Communication Engineering, College of Engineering, Guindy, Anna University, Chennai 600025, India*

[2]*Department of Electronics and Communication Engineering, Sri Sivasubramaniya Nadar College of Engineering, Kalavakkam, Chennai 603110, India*

[3]*Department of Electronics and Communication Engineering, SRM Institute of Science and Technology, Chennai, Tamilnadu, India*

Correspondence should be addressed to Malathi Kanagasabai; mala@annauniv.edu

The proposed work is a novel low-profile 5G MIMO antenna configuration to exhibit dual-band frequencies for 5G NR-n2 band (1.9 GHz) and safety band (ITS-5.9 GHz) in vehicular communication. In the proposed antenna, it is quite difficult to achieve the lowest resonance frequency in a comparatively miniaturized dimension concerning its operating wavelength. The designed antenna is a modified square patch with the dual-band resonance achieved by the incorporation of slots for increasing the electrical length within the dimension. Hence, the design comprises ring and loop slots exhibiting resonance at 1.9 GHz and the loop U, and modified-W slots for 5.9 GHz. The antenna achieves 1.9% and 0.64% impedance bandwidth and a peak gain of 1.944dBi and 6.06dBi at the resonant frequencies of 1.9 GHz and 5.9 GHz, respectively, with dimensions of $0.114\lambda o \times 0.114\lambda o \times 0.0016\lambda o$, where λo is the wavelength of the lowest operating frequency. The MIMO configuration is presented to assess the antenna's suitability for large-scale applications. The MIMO antenna presented here is deployed with the edge-to-edge distance between the single element radiators being $0.01\lambda o$ by parametric sweep. The presented MIMO antenna provides an isolation value greater than 19 dB because of reduced mutual coupling between the single element radiators in that MIMO structure due to the presence of a ground slot. The ECC values are 1.659×10^{-9} and 0.000601 for frequencies of 1.9 GHz and 5.9 GHz, respectively, and the diversity gain is relatively near 10 dB, which is the acceptable value for MIMO antennas. This modified square single-element and MIMO antenna provides a relatively higher gain and better performance in vehicular communication for GSM and safety applications. The MIMO configurations' on-vehicle analysis is performed to check the reliability of the designed antenna in a vehicular environment.

1. Introduction

At present, most emerging applications, such as the Internet of things, vehicular communication, navigation systems, and mobile communication, use 5G microwave as well as millimeter-wave frequencies for signal transfer. The next generation of technology will offer higher capacity, extremely low latency, extremely high data rates, and exceptional service quality. It is important to note that the advent of 5G technology will open new doors for development that have previously been closed. Due to 5G technology's support for IoT, huge societal changes in the realms of business, healthcare, and other social sectors are possible. Many linked devices are anticipated to be made possible by 5G technology, and by maintaining a trade-off between speed, cost, and latency, a network will be able to meet the communication needs [1].

The demand for distinctive antenna structures comprises antennas with some attractive features such as low-profile,

compact size [2], and requiring wide operating bandwidth [3–5], which are added requirements nowadays [6–9]. Hence, designing an antenna that includes the above-mentioned prominent features is to be designed. In vehicular communication, both the sub-6 GHz [10, 11] and millimeter-wave frequencies [12] of 5G have become renowned bands of operation as all other technologies move towards 5G technology for communications. This vehicular communication radiator uses an Unlicensed National Information Infrastructure (U-NII-4) of 5.9 GHz for establishing communication in a vehicle-to-network (V2N) platform, which increases road safety and traffic efficiency. Also, the 5G NR-n2 band is specially allocated for personal communication services used for vehicle-to-network communication.

A regular microstrip patch antenna can be used for 5G, but it exhibits a narrow bandwidth due to the reduction in antenna size. To improve the bandwidth of the antenna, some of the techniques such as stacking substrate, meta-surface [13], thick, low permittivity substrate, shorting pins [14, 15], slots and slits [15–17], crossing stub structure [16], and folded patch [17], are used but with a lateral increase in size, volume, and cost of fabrication. One of the methods to improve bandwidth is using microstrip line and proximity feeding techniques with the meta-surface antenna [13] for 5 GHz frequency band excitation with an improved bandwidth, but the antenna size is comparatively large for a single-band antenna. Coupled microstrip line patch is also used with the gap loading technique [14] to reduce the antenna size and obtain low-frequency [18]. Another method for improving bandwidth is etching slots of different shapes, such as V-slot [15], elliptical slot [19], and U-slot [17], in the antenna. In [20], the substrate integrated irregular ground (SIIG) structure with connected vias is designed using a technique of plated-through hole, providing a reduction in its footprint of 75.6% and also to stabilize the frequency, the patch is sliced into small square patches [21].

In vehicular communication, vehicles will play a crucial role in the communications of the modern era, which promises to offer ubiquity, ultra-reliability, and cheap cost [22–24]. Instead of attempting to alter the current communications architecture, 5G offers a platform that unifies all currently used and future-proofed technologies to supply clients with a wide range of services [25]. The antenna to be placed on the surface of the vehicle should be compact. Hence, miniaturization of the antenna is proposed by using techniques such as using high permittivity substrate and irregular ground plane [20], but it is expensive and complex. Because of these consequences, low-profile and single-layer antennas are proposed [3, 13, 14, 19–21]. The automotive application supports various services at different frequency ranges and requires a separate antenna for operation, which leads to the crowding of antennas on the vehicle surface [26]. This reduces the antenna performance on account of interference. To subdue this drawback, dual-band or wideband [27] antennas are proposed. The number of antennas performing different services is reduced. The techniques used for dual-band are structure sharing, shared aperture, coupled microstrip lines [14], and stacking of substrate, and liquid crystal polymer [28] is used as the substrate to obtain multiband.

Other than the above constraints in vehicular communication, the gain and efficiency of the antenna also play a vital role, which can be improved by implementing MIMO [29, 30]. The MIMO configuration of the antenna exhibits increased mutual coupling due to its spacing between antenna elements, which reduces isolation. Traditionally, the distance between the elements is kept at half the wavelength. In recent periods, various studies of MIMO isolation augmentation have been conducted. Numerous decoupling methods like defective ground structures, parasitic scatterers, wideband neutralization lines, beamforming networks, metamaterials [31–33], reactively loaded elements, characteristic modes, and others are available for 2 or 4 MIMO antennas. Some of the techniques that are used to improve isolation in the literature include separate isolation structures [34], etching slits [35, 36], and slots [37, 38] on the ground and adding decoupling devices [39, 40]. The isolation structure used in [34] consists of a two-proximity coupled fed microstrip square ring patch antenna and two quarter-wavelength microstrip slot antennas, which are printed on different sides to reduce mutual coupling, which in turn reduces the isolation. The MIMO antenna in [39] uses decoupling devices such as a winding branch of resonance, a modified serpentine structure [41], and a reversed T-slot etched in-ground for better isolation, but the size is larger for compact antennas.

In this paper, a compact low-profile dual-band antenna operating at the frequencies of 1.9 GHz 5G NR-n2 band and 5.9 GHz safety band for vehicular communication is proposed. The dimension of the antenna proposed is $0.114\lambda0 \times 0.114\lambda0 \times 0.0016\lambda0$ and the antenna size is reduced to $0.125\lambda0$. The single-layer substrate of Rogers RT-5870 dielectric of permittivity (εr) 2.33 is used. The impedance bandwidth is 1.9% and 0.64% and the antenna gains are 1.94 dBi and 6.06 dBi for the operating frequencies of 1.9 GHz and 5.9 GHz, respectively. The MIMO configuration for the proposed antenna is designed and its characteristics are analyzed. In this manuscript, the sections are organized as follows: the presented antenna design is in Section 2. In Section 3, the results and discussions for the designed antenna are stated. The onboard analysis for the vehicular application is described in Section 4, followed by the conclusion and references in Section 5.

2. Antenna Design

The construction of the proposed single-layer antenna is shown in Figure 1. The radiating patch is embedded above the thin dielectric substrate Rogers RT-5870 of permittivity εr = 2.33, loss tangent 0.0012, and thickness 0.254 mm. The overall dimensions of the proposed antenna are $0.114\lambda0 \times 0.114\lambda0 \times 0.0016\lambda0$, where $\lambda0$ is the free-space wavelength at the lowest resonating frequency of 1.9 GHz. The radiating patch is fed with a coaxial probe along the surface parallel to the y-axis, which is represented as a feed line in Figure 1(c). The proposed antenna's coaxial feed inner conductor is placed over the top radiating element PEC of the antenna and soldered. While the outer conductor of the coaxial feed is adjoined with both the top radiating
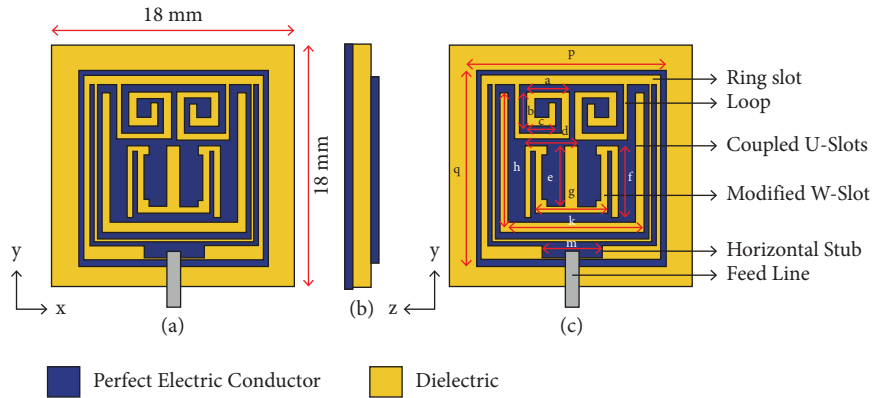
FIGURE 1: Configuration of the proposed square patch antenna with material definitions. (a) Front view, (b) side view, and (c) geometrical details and labels of the proposed antenna: $a = 3.18$ mm, $b = 2.55$ mm, $c = 2.15$ mm, $d = 4.03$ mm, $e = 4.5$ mm, $f = 5.4$ mm, $g = 5.5$ mm, $h = 10.45$ mm, $k = 10.9$ mm, and $m = 4.4$ mm.

element and the bottom ground plane of the proposed antenna. This exhibits a size reduction of $0.125\lambda0$ from the actual antenna wavelength of $0.5\lambda0$.

2.1. Design of Dual-Band Antenna.

The fundamental parameter to obtain the resonance at a lower frequency is the electrical length of the stubs in the radiator, i.e., by increasing the inductive effect. For a better understanding of the designed patch antenna, the labels and physical dimensions are shown in Figure 1(c). Hence, various techniques are used to increase this inductive effect. The detailed structural evolution process of the antenna is explained in the next section. Here, the proposed antenna exhibits the reflection coefficient characteristics below −10 dB obtained from simulation as pictured in Figure 2. The low-frequency resonance is because of the increased coupling effect of the outer slots, whereas the higher frequency resonance is obtained by the coupling effect of the slots in the midpart of the radiator. The bandwidth of each band depends on the overall size of the slots and stubs used in the patch antenna. The higher frequency covers a band of (5.90 GHz–5.94 GHz) 0.64% and the lower frequency covers a band of up to (1.88 GHz–1.92 GHz) 1.9%.

2.2. Evolution of Antenna with S-parameters.

The proposed antenna design is initiated with a square patch as shown in Figure 3(a) (STAGE-1). A ring-shaped slot is added in the square patch to provide the resonance at 8 GHz with less impedance matching than in STAGE-2. In STAGE-3, the meandering technique is incorporated by inserting a loop-shaped slot to increase the electrical length of the designed antenna, shifting the frequency to 1.9 GHz. This is due to the inductive effect caused by the electrical length enhancement by each curve of the loop. To counteract this effect of the antenna, a coupled U-shaped slot is added in between the loop and the ring for coupling purposes, which introduces another band around frequency 2.6 GHz.

This coupled U-slot is the combination of an asymmetrical U-slot and a thin U-slot, which helps in increasing the coupling between the slots by the step-
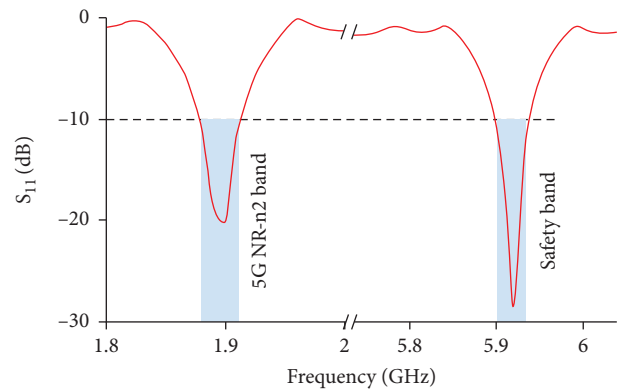

FIGURE 2: Simulated reflection characteristics of the proposed antenna design are represented with their respective band applications.

impedance matching technique. Two inverted U-slots are added at the center, as shown in STAGE-4. To attain the desired excitation frequencies, the inverted U-slots are converted into a modified W-slot in STAGE-5, which resonates at 1.9 GHz and 5.9 GHz. To prevent that capacitance effect at a higher frequency, a stub that induces the inductance effect is added. Finally, at STAGE-6, two vertical rectangular stubs are added to the inverted U-slots and a horizontal rectangular stub to the bottom side of the ring. Normally, a patch antenna exhibits a narrow bandwidth when the size of the antenna is reduced. Here, the bandwidth of the frequencies is improved by those stubs. The simulated reflection characteristic of each stage of the proposed antenna is depicted in Figure 3(b). The dual-band response and bandwidth of the proposed antenna are controlled by the respective slots incorporated in the modified square patch as mentioned in the evolution.

2.3. Proposed MIMO Antenna Design.

To improve the performance characteristics of the proposed antenna design, MIMO configuration is implemented. In this, the separation of antenna elements is fixed by using the parametric sweep
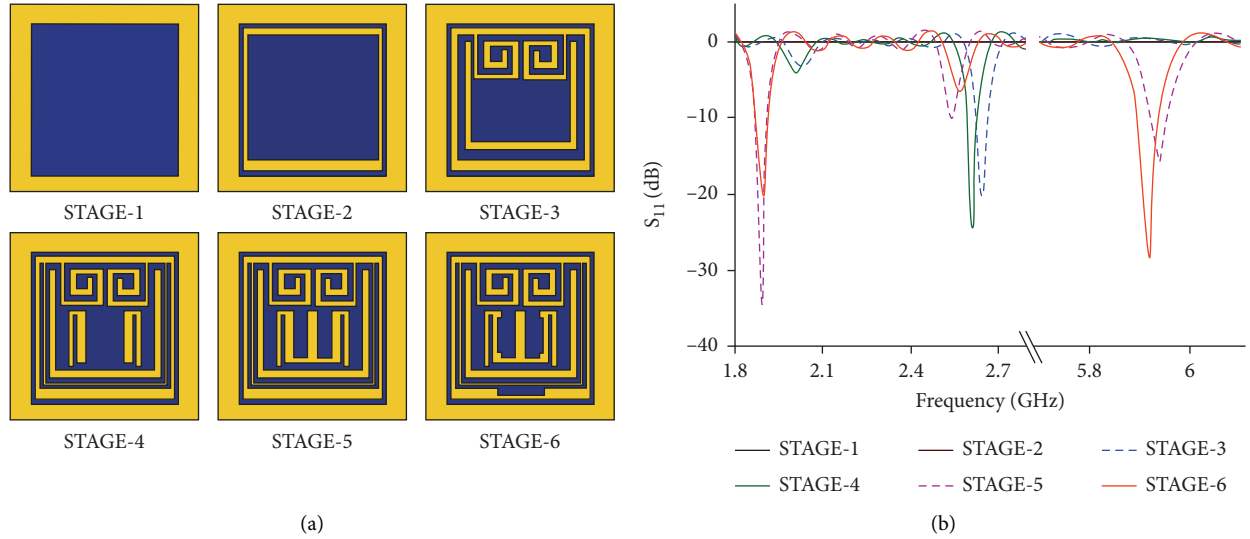
FIGURE 3: Designed antenna's evolution represented as (a) STAGE-1 square patch, STAGE-2 square patch with ring slot, STAGE-3 patch with the ring, loop slot, and coupled U-slot, STAGE-4 with added inverted U-slots, STAGE-5 with extended W-slots, STAGE-6 final patch with all slots and horizontal stub. (b) Reflection characteristics for the respective evolution changes.
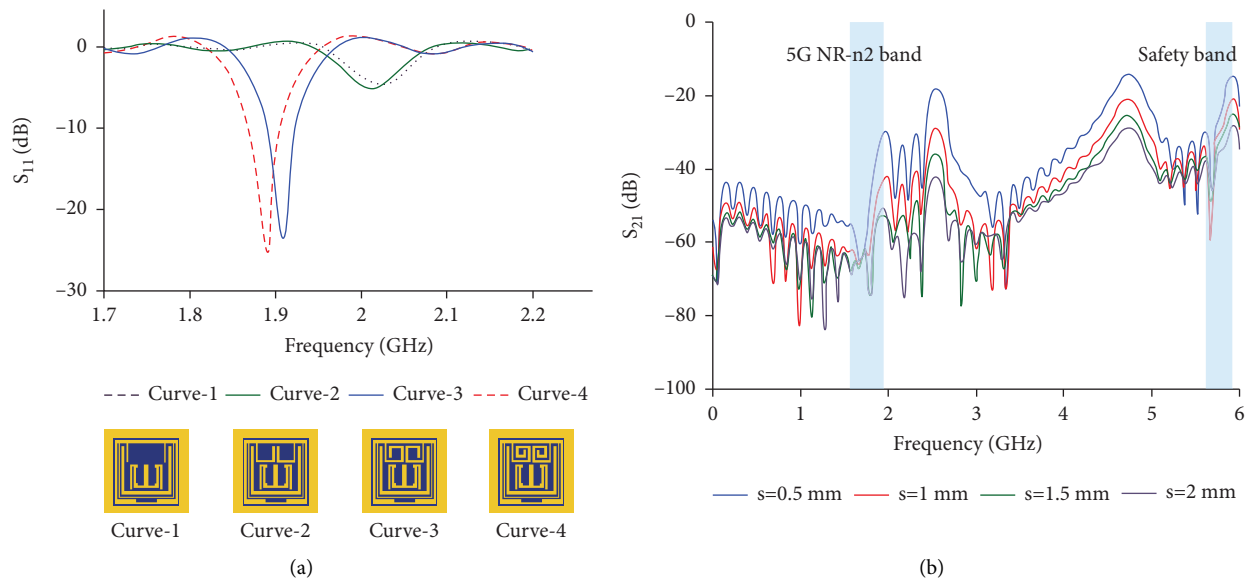

FIGURE 4: Parametric analysis. (a) Loop present in the upper end of the top radiating patch. The lower frequency of 1.9 GHz is obtained as the electrical length of the loop increases for every curve. (b) Spacing changed from 0.5 to 2 mm with their respective isolation characteristics.

technique as shown in Figure 4(b). With this, the performance characteristics of various spacing values are simulated, and $s = 1.5$ mm is fixed based on the reflection and isolation characteristics exhibited by the antenna. The designed MIMO antenna and its isolation characteristics are shown in Figures 5(a) and 5(b). This MIMO antenna isolation value exceeds 19 dB as there is defective ground structure [37, 38] between the two single-element radiators placed adjacent to one another. The gain of the MIMO antenna is relatively larger compared to that of the single element antennas. The MIMO antenna gains are 2.93 dBi and 6.18 dBi for frequencies of 1.9 GHz and 5.9 GHz, respectively.

3. Results and Discussions

The proposed antenna is fabricated and measured to validate the results obtained from the CST Studio simulation. The measurement setup of the fabricated prototype contains Agilent's Vector Network Analyzer which is shown in Figure 6(a) and the radiation pattern measurements are carried out in an anechoic chamber shown in Figure 6(b) with the input power of 20 dBm.

3.1. S-parameters Comparison. The simulated and measured reflection characteristics of the fabricated single-element radiator are plotted and compared. The obtained results
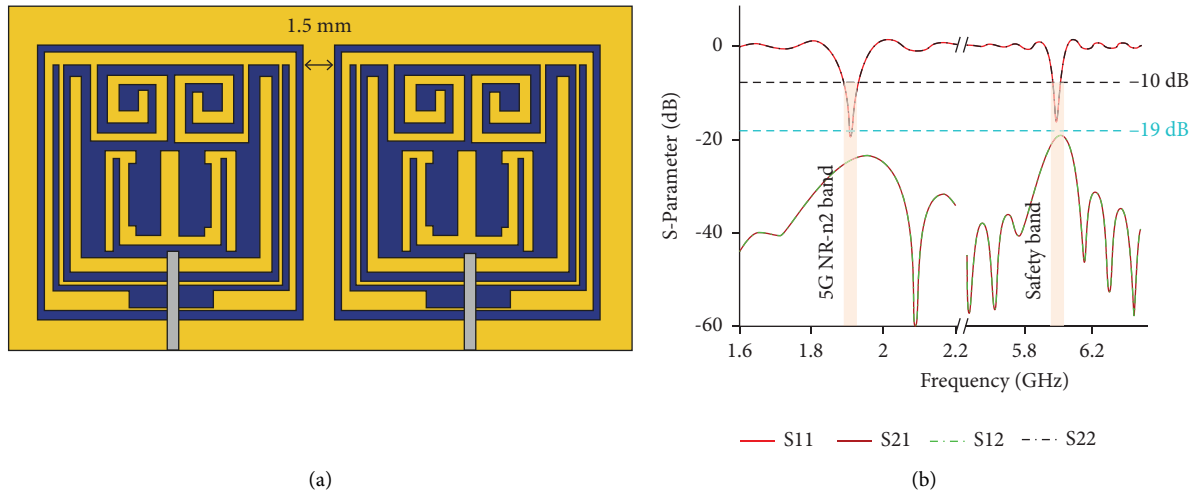
(a)

(b)

FIGURE 5: (a) Configuration of the proposed single element modified square patch antenna design placed adjacent to each other with a spacing obtained from parametric sweep 1.5 mm. (b) Simulated reflection and isolation characteristics of proposed two-port MIMO antenna design.

cover the required operating frequencies as depicted in Figure 7(a). The disparity between the simulated and measured S11 in the resonant frequencies is due to the soldering of the SMA connector and tolerance of manufacture [39]. In a two-port MIMO antenna design, an isolation value of greater than 19 dB is exhibited by both the simulated and measured characteristics, which are shown in Figure 7(b). The radiation pattern of the designed antenna structure exhibits a directional radiation pattern for the operating frequencies. The simulated and measured radiation patterns for the YZ-plane and XZ-plane are shown in Figure 8.

3.2. Single Element Antenna—Performance Analysis. The surface current density determines the region of maximum current flow for that specific resonant frequency. The induced current distribution over the radiator is illustrated in Figure 9. The current flow in the region where the loop and ring slot are coupled exhibits a lower frequency (1.9 GHz), and the current flow at the coupled U-slot, loop, and modified W-slot exhibits the higher frequency (5.9 GHz). The gain and total efficiency value of the proposed antenna are shown in Figure 10. The simulated gain is 1.94 dBi for 1.9 GHz and 6.06 dBi for 5.9 GHz, respectively. The radiation and total efficiencies of the proposed antenna for the frequencies are 80.5% and 88.3% for the 5G NR-n2 band and 83.3% and 90.1% for the safety band, respectively.

3.3. MIMO Antenna—Performance Analysis. Diversity gain determines the signal strength of the MIMO antenna by comparing the signal gathered by the desired antenna element with the signal gathered by the combination of other antenna elements, which is used to evaluate the performance of the MIMO antenna. By the postprocessing method, the simulated diversity gain of the proposed MIMO antenna is analyzed and found to be nearly equal to 10 dB, which is the

required value. Another major performance characteristic of the MIMO antenna is the envelope correlation coefficient (ECC), which determines how the antenna pattern is independent of one another. The acceptable ECC value for the MIMO antenna is less than or equal to 0.3. The ECC values of the proposed antenna are also calculated using the postprocessing method in CST, where the value is 1.659×10^{-9} and 0.000601 for frequencies of 1.9 GHz and 5.9 GHz, respectively. On comparing the proposed model with the previous works of literature, the MIMO configuration exhibits better isolation characteristics as expected because some of the previous models use separate isolation PEC structures [34] and decoupling devices [39], but this model provides good isolation than the literature without any additional isolation structures in the radiator. A link budget assesses a communication system's performance while considering all the losses that a communication link experiences. Here the MIMO antenna link budget is calculated for the operating frequencies of 1.9 GHz and 5.9 GHz. The received power is calculated using the method in [42]. However, for metropolitan areas, the Federal Communication Commission and the World Health Organization advise antenna power of up to 30 dBm. V2X communication is subject to a 21 dBm transmission power limit set by the 5G Automotive Association (5GAA). Hence, the values are plotted for 21 dBm and 30 dBm power in the resonant frequencies of 1.9 GHz and 5.9 GHz. As per the noise margin obtained as mentioned in [42], the proposed antenna provides a 1.25 km and 1.15 km link for the transmit power of 21 dBm as represented in Figure 11, which is better than the 0.3 km requirement set by the 5G Automotive Association.
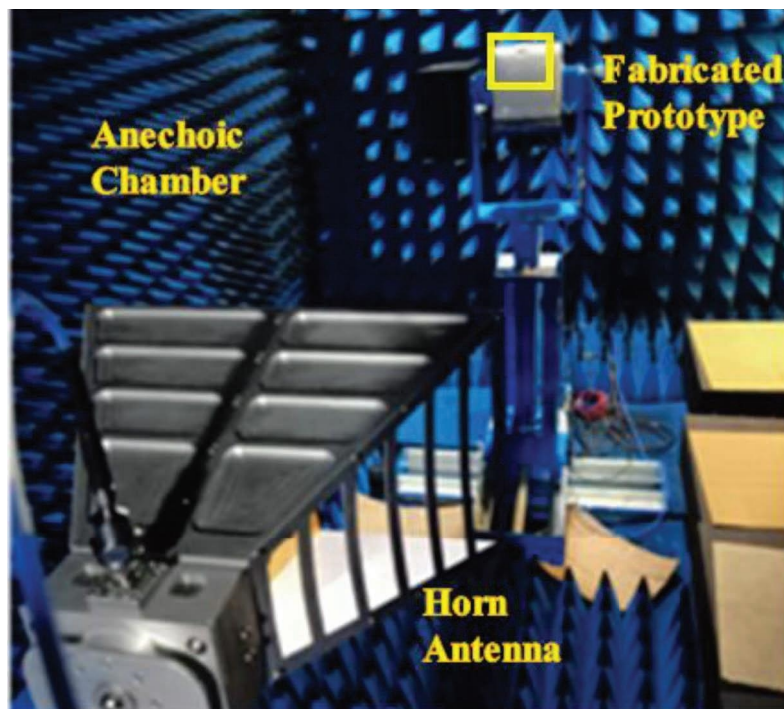
4. Onboard Analysis

To study more about the antenna performance after its placement in the car, computational modeling is carried out as shown in Figure 12. Some of the factors that inhibit the
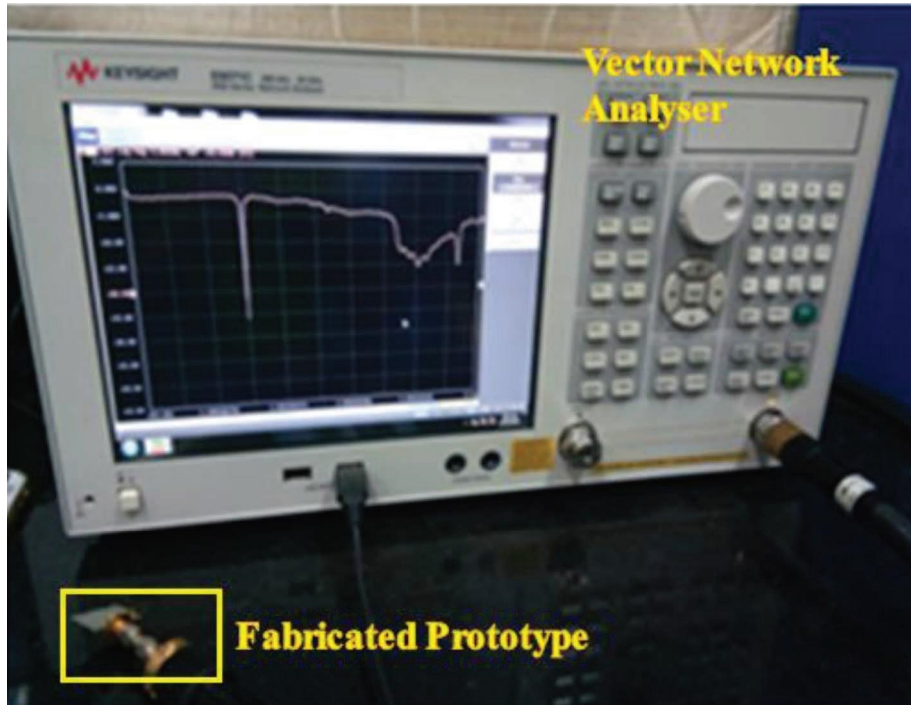
(a)

(b)

FIGURE 6: Measurement setup of the proposed antenna. (a) Agilent's Vector Network Analyzer for the S-parameter measurements. (b) Anechoic chamber for radiation pattern.

performance of the antenna are placement of the antenna, material of the car model, obstacles around the antenna, etc. The source is placed in the shark fin of the vehicle where the losses due to the reflections of the car surfaces are less and the miniaturized antenna profile is well suited. The far-field radiation characteristic of the integrated antenna is analyzed using the CST Software Studio, which will reduce the experimental cost and optimize the antenna placement to improve the overall performance. The CAD model of the car is incorporated into the CST and the far-field sources of the
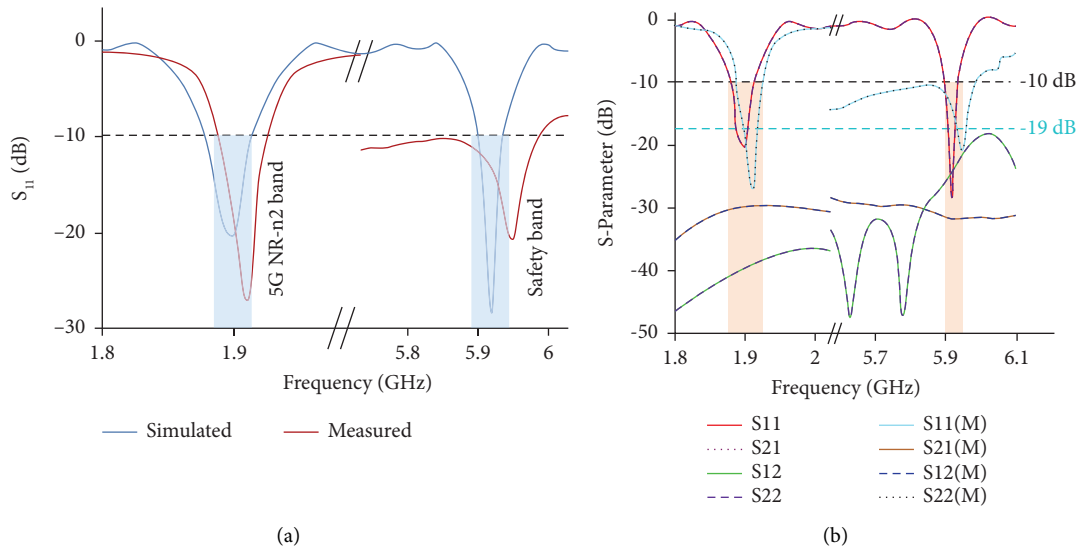
(a)

(b)

FIGURE 7: Simulated and measured reflection coefficient characteristics of the proposed simulated antenna design and fabricated prototype. (a) Single element. (b) MIMO, where the M in the legend represents the measured value.
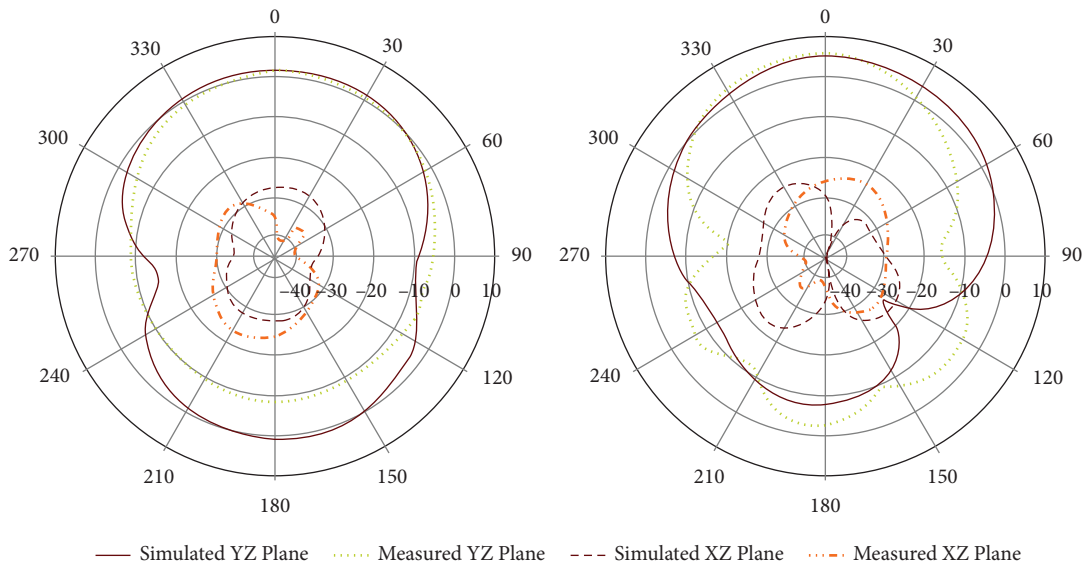

FIGURE 8: Simulated and measured radiation pattern for both the horizontal plane and vertical plane (a) 1.9 GHz (b) 5.9 GHz.

respective operating frequencies of the presented antenna are analyzed. The simulated far-field patterns of the on-vehicle analysis for 1.9 GHz and 5.9 GHz are shown in Figure 12.

The proposed antenna design has the following prominent features contributing to its novelty:

(1) An undemanding antenna structure with modified slots in the basic square patch is proposed. This requires a very simple fabrication procedure and is less expensive.

(2) The presented antenna does not involve highly stacked layers as in [20] and other structures such as shorting vias and active components.

(3) The designed radiator is layered over a dielectric Rogers RT5870 substrate, which offers low electric loss and very low thickness and is highly ideal for high-moisture environments compared to the other substrates used in [20, 27, 34].

(4) This slot incorporated square patch antenna provides a dual-band for the 5G new radio n2 band and a safety band for vehicular communications unlike the other complex structures for single-band antenna [14, 16, 21].

(5) The depicted antenna's gain and efficiency have better values compared to the existing art of literature [27].
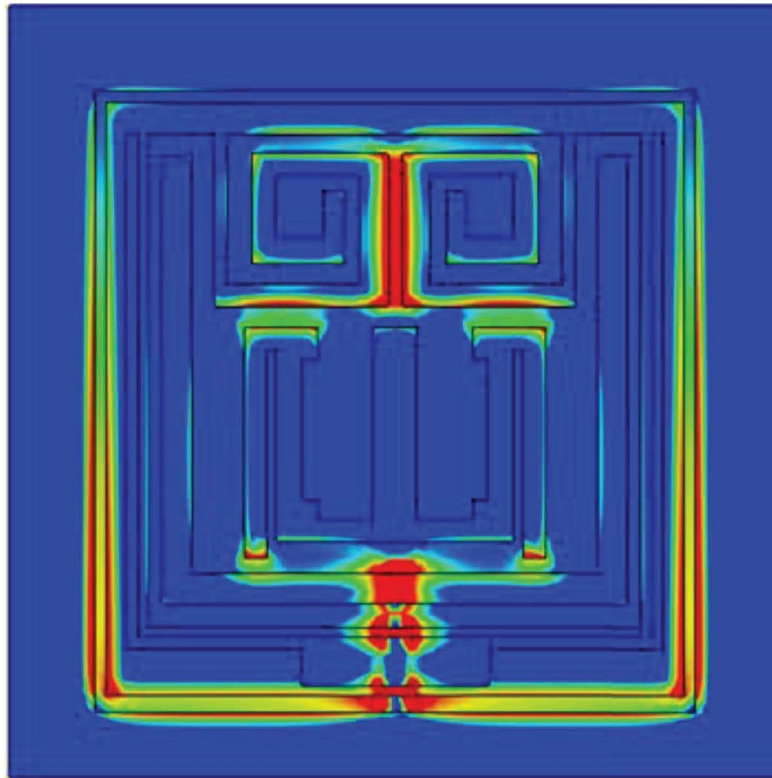
(a)
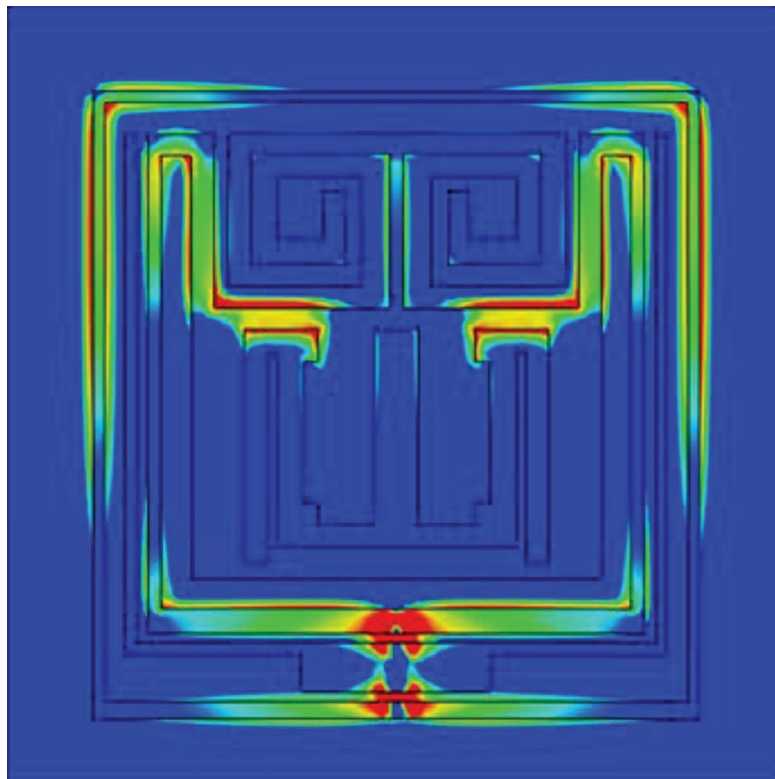
(b)

FIGURE 9: Surface current distribution of the proposed antenna for frequencies (a) 1.9 GHz (b) 5.9 GHz.

(a)

(b)
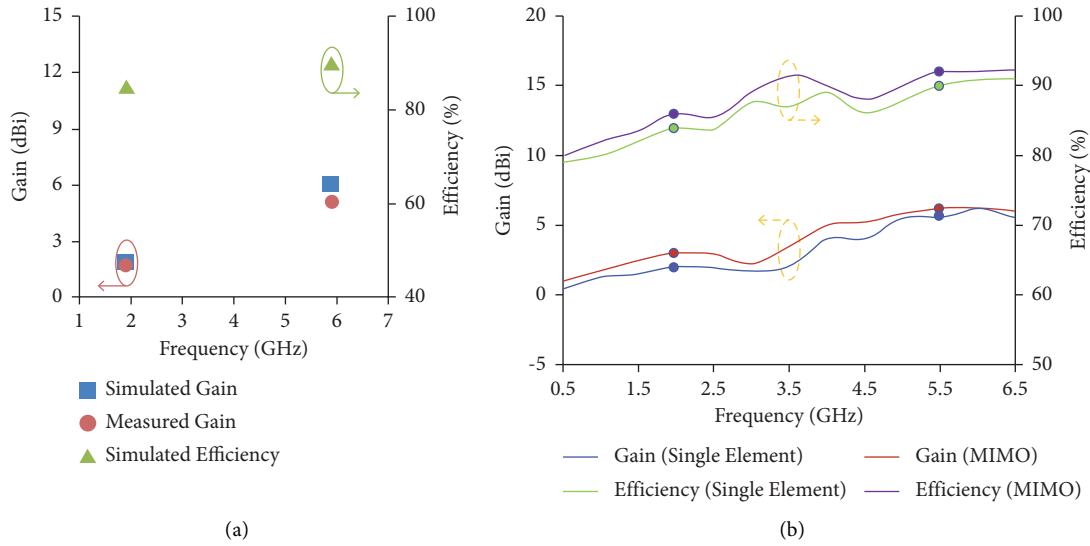
FIGURE 10: (a) Simulated gain and efficiency and measured gain of the proposed modified square patch antenna are compared in the plot. (b) 2D gain and efficiency curve of the single element and array antennas are plotted and compared.

(a)

(b)

FIGURE 11: Link budget of the proposed MIMO antenna for the operating frequencies. (a) 1.9 GHz and (b) 5.9 GHz.

(a)

(b)

FIGURE 12: Far-field radiation pattern of the integrated antenna on the CAD model of car. (a) 1.9 GHz (b) 5.9 GHz.

TABLE 1: Comparison of the proposed antenna with existing antennas in literature.

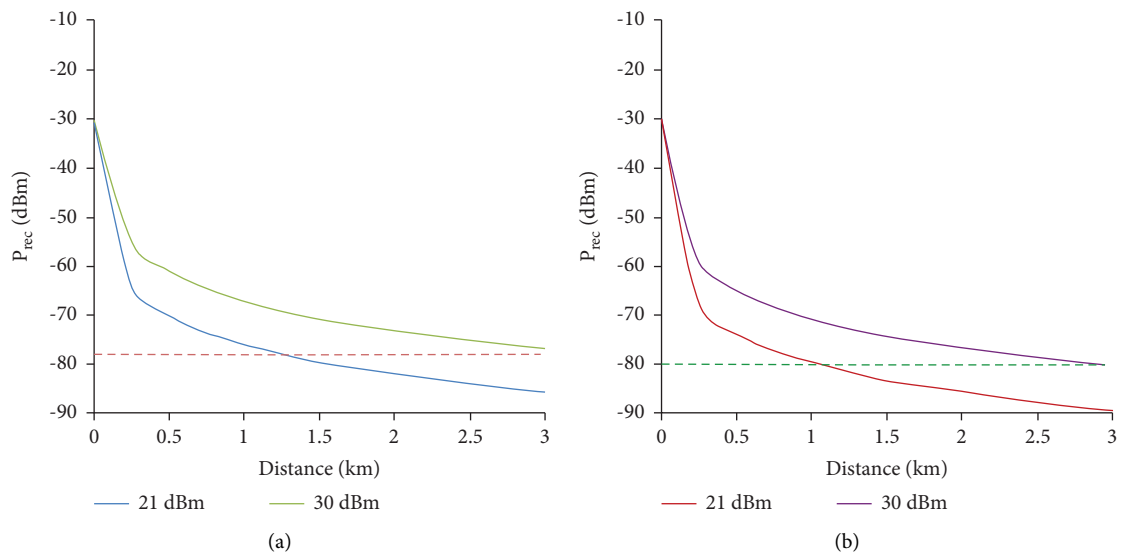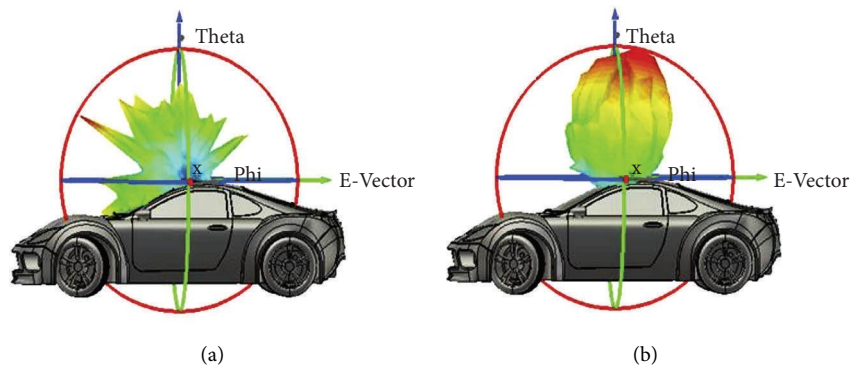| Ref.no	Frequency (GHz)	Dimension (mm^3)	Gain (dBi)	Bandwidth	Efficiency (%)	Isolation (dB)	No. of array	Distance between array elements	Design complexity
[37]	2.45 3.1–10.6	30 × 40 × 0.8	—	—	77.5	10	2	6.4 mm	Meandering monopole antenna
[34]	2.4	0.64λ × 0.48λ	2.3	0.9 GHz	—	25	2	—	Isolation structure etched on the ground plane
[43]	3.55	0.29λ × 0.29λ	8.5	0.3 GHz	—	35	2	60 mm	Spacing is very large that leads to larger MIMO structure.
[44]	3.5	140 × 70 × 0.97	5	12%	50%	10	2	10.4 mm	Multiple inverted-F antennas (IFAs) on an artificial magnetic conductor (AMC) ground
[39]	2.4/5	77.5 × 52 × 1.6	—	0.08/ 0.675 GHz	77%	15	2	0.115λo	Two symmetrical winding inverted-F antenna and two decoupling devices for isolation
[41]	2.45	30 × 30 × 1.6	—	0.05 GHz	—	10	2	6 mm	Modified serpentine structure with decoupling structures
This work	1.9 5.9	18 × 18 × 0.254	2.93 6.18	1.9% 0.64%	88.3% 90.1%	18	2	1.5 mm	Reduced antenna size, high gain, and efficiency

(6) The onboard analysis signifies that the designed antenna does not have any noticeable performance reduction in real-time applications. Table 1 compares the proposed work with previous literature.

5. Conclusion

Thus, a low-profile antenna operating at dual-band 1.9 GHz of 5G NR-n2 band and 5.9 GHz of safety band is proposed. The slots and stubs are used to achieve the lower resonant frequency and to improve bandwidth. The presented antenna, of dimensions 0.114λo × 0.114λo × 0.0016λo, achieves 1.9% and 0.64% impedance bandwidth and peak gains of 1.944 dBi and 6.06 dBi at the resonant frequencies of 1.9 GHz and 5.9 GHz, respectively. The S-parameter and radiation pattern of corresponding frequencies are simulated and compared with measured results obtained from the fabricated prototype. To improve performance, the single elements in the MIMO antenna design are spaced 0.01λo, which exhibits better isolation of 18 dB in the two-port configuration. The diversity gain of 10 dB and ECC values of less than 0.3 are obtained for the proposed design with the requirements. The antenna size is reduced by about 0.125λ0 from 0.5λ0 when compared with the previous kinds of literature, which can be suitable for the various vehicular communication services. The overall size reduction, performance enhancement, and MIMO deployment make the proposed antenna reliable and versatile in vehicular communication areas.

Data Availability

The data used or analysed during the study can be obtained from the corresponding author upon request.

Conflicts of Interest

The authors declare that they have no conflicts of interest.

References

[1] S. Kumar, A. S. Dixit, R. R. Malekar, H. D. Raut, and L. K. Shevada, "Fifth generation antennas: a comprehensive review of design and performance enhancement techniques," *IEEE Access*, vol. 8, pp. 163568–163593, 2020.

[2] A. Ameelia Roseline and K. Malathi, "Compact dual-band patch antenna using spiral shaped electromagnetic bandgap structures for high speed wireless networks," *AEU - International Journal of Electronics and Communications*, vol. 66, no. 12, pp. 963–968, 2012.

[3] C. L. Mak, H. Wong, and K. M. Luk, "High-gain and wideband single-layer patch antenna for wireless communications," *IEEE Transactions on Vehicular Technology*, vol. 54, no. 1, pp. 33–40, Jan. 2005.

[4] S. K. Palaniswamy, M. Kanagasabai, S. Arun Kumar, M. G. N. Alsath, S. Velan, and J. K. Pakkathillam, "Super wideband printed monopole antenna for ultra wideband applications," *International Journal of Microwave and Wireless Technologies*, vol. 9, no. 1, pp. 133–141, 2017.

[5] S. Kingsly, D. Thangarasu, M. Kanagasabai et al., "Tunable band-notched high selective UWB filtering monopole antenna," *IEEE Transactions on Antennas and Propagation*, vol. 67, no. 8, pp. 5658–5661, 2019.

[6] D. Garrido Lopez, M. Ignatenko, and D. S. Filipovic, "Low-profile tri-band inverted-F antenna for vehicular applications in HF and VHF bands," *IEEE Transactions on Antennas and Propagation*, vol. 63, no. 11, pp. 4632–4639, Nov, 2015.

[7] S. A. Sanghai, M. Ignatenko, and D. S. Filipovic, "Low-profile two-arm inverted-L antenna design for vehicular HF communications," *IEEE Transactions on Antennas and Propagation*, vol. 65, no. 11, pp. 5710–5719, 2017.

[8] S. Mohandoss, S. K. Palaniswamy, R. R. Thipparaju, M. Kanagasabai, B. R. Bobbili Naga, and S. Kumar, "On the bending and time domain analysis of compact wideband flexible monopole antennas," *AEU - International Journal of Electronics and Communications*, vol. 101, pp. 168–181, 2019.

[9] M. Alibakhshi-Kenari, A. Andújar, and J. Anguera, "New compact printed leaky-wave antenna with beam steering," *Microwave and Optical Technology Letters*, vol. 58, no. 1, pp. 215–217, 2016.

[10] M. Alibakhshikenari, B. S. Virdee, C. H. See et al., "Dual-polarized highly folded bowtie antenna with slotted self-grounded structure for sub-6 GHz 5G applications," *IEEE Transactions on Antennas and Propagation*, vol. 70, no. 4, pp. 3028–3033, 2022.

[11] M. Alibakhshikenari, S. M. Moghaddam, A. Uz Zaman, J. Yang, B. S. Virdee, and E. Limiti, "Wideband sub-6 GHz self-grounded bow-tie antenna with new feeding mechanism for 5G communication systems," in *Proceedings of the 2019 13th European Conference on Antennas and Propagation (EuCAP)*, pp. 1–4, Krakow, Poland, March 2019.

[12] M. Alibakhshikenari, B. S. Virdee, A. A. Althuwayb et al., "Study on on-chip antenna design based on metamaterial-inspired and substrate-integrated waveguide properties for millimetre-wave and THz integrated-circuit applications," *Journal of Infrared, Millimeter and Terahertz Waves*, vol. 42, no. 1, pp. 17–28, 2021.

[13] J. d. D. Ntwangaheza, L. Sun, Z. Xie, Y. Pang, Z. Zheng, and G. Rushingabigwi, "A single-layer low-profile broadband metasurface antenna array for sub-6 GHz 5G communication systems," *IEEE Transactions on Antennas and Propagation*, vol. 69, no. 4, pp. 2061–2071, 2021.

[14] Z. Shao and Y. Zhang, "A single-layer miniaturized patch antenna based on coupled microstrips," *IEEE Antennas and Wireless Propagation Letters*, vol. 20, no. 5, pp. 823–827, 2021.

[15] H. Wong, K. K. So, and X. Gao, "Bandwidth enhancement of a monopolar patch antenna with V-shaped slot for car-to-car and WLAN communications," *IEEE Transactions on Vehicular Technology*, vol. 65, no. 3, pp. 1130–1136, 2016.

[16] W.-H. Zhang, Q. Xue, S. Liao, W. Che, and W. Yang, "Low-profile compact microstrip magnetic dipole antenna with large beamwidth and broad bandwidth for vehicular applications," *IEEE Transactions on Vehicular Technology*, vol. 70, no. 6, pp. 5445–5456, June 2021.

[17] C. Y. Chiu, K. Man Shum, C. H. Chan, and K. Man Luk, "Bandwidth enhancement technique for quarter-wave patch antennas," *IEEE Antennas and Wireless Propagation Letters*, vol. 2, pp. 130–132, 2003.

[18] P. Sambandam, M. Kanagasabai, R. Natarajan, M. G. N. Alsath, and S. Palaniswamy, "Miniaturized button-like WBAN antenna for off-body communication," *IEEE Transactions on Antennas and Propagation*, vol. 68, no. 7, pp. 5228–5235, July 2020.

[19] X. Li and C. Du, "Compact triple-band Liquid crystal polymer based flexible antenna for WiMAX/WLAN/5G applications," in *Proceedings of the 2019 International Workshop on Electromagnetics: Applications and Student Innovation Competition (iWEM)*, pp. 1-2, Qingdao, China, September 2019.

[20] W. An, Y. Li, H. Fu, J. Ma, W. Chen, and B. Feng, "Low-profile and wideband microstrip antenna with stable gain for 5G wireless applications," *IEEE Antennas and Wireless Propagation Letters*, vol. 17, no. 4, pp. 621–624, 2018.

[21] J. d. D. Ntwangaheza, L. Sun, Y. Li, D. Biao, Z. Xie, and G. Rushingabigwi, "A single-layer planar low-profile wideband microstrip line-fed metasurface antenna," *IEEE*

[22] Y. Hua, L. Huang, and Y. Lu, "A compact 3-port multiband Antenna for V2X communication," in *Proceedings of the 2017 IEEE International Symposium on Antennas and Propagation & USNC/URSI National Radio Science Meeting*, pp. 639-640, CA, USA, July 2017.

[23] B. Feng, J. Chen, S. Yin, C.-Y.-D. Sim, and Z. Zhao, "A tri-polarized antenna with diverse radiation characteristics for 5G and V2X communications," *IEEE Transactions on Vehicular Technology*, vol. 69, no. 9, pp. 10115–10126, Sept. 2020.

[24] M. G. N. Alsath and M. Kanagasabai, "Planar pentaband Antenna for vehicular communication application," *IEEE Antennas and Wireless Propagation Letters*, vol. 13, pp. 110–113, 2014.

[25] S. A. A. Shah, E. Ahmed, M. Imran, and S. Zeadally, "5G for vehicular communications," *IEEE Communications Magazine*, vol. 56, no. 1, pp. 111–117, Jan. 2018.

[26] M. G. N. Alsath, H. Arun, Y. P. Selvam et al., "An integrated tri-band/UWB polarization diversity antenna for vehicular networks," *IEEE Transactions on Vehicular Technology*, vol. 67, no. 7, pp. 5613–5620, 2018.

[27] M. O. Khalifa, A. M. Yacoub, and D. N. Aloi, "A multi-wideband compact antenna design for vehicular sub-6GHz 5G wireless systems," *IEEE Transactions on Antennas and Propagation*, vol. 69, no. 12, pp. 8136–8142, 2021.

[28] D. Wang, H. Wong, and C. H. Chan, "Small patch antennas incorporated with a substrate integrated irregular ground," *IEEE Transactions on Antennas and Propagation*, vol. 60, no. 7, pp. 3096–3103, 2012.

[29] M. Ikram, N. Nguyen-Trong, and A. Abbosh, "Multiband MIMO microwave and millimeter antenna system employing dual-function tapered slot structure," *IEEE Transactions on Antennas and Propagation*, vol. 67, no. 8, pp. 5705–5710, 2019.

[30] X. L. Liu, Z. D. Wang, Y. Z. Yin, J. Ren, and J. J. Wu, "A compact ultrawideband MIMO antenna using QSCA for high isolation," *IEEE Antennas and Wireless Propagation Letters*, vol. 13, pp. 1497–1500, 2014.

[31] M. Alibakhshikenari, B. S. Virdee, L. Azpilicueta et al., "A comprehensive survey of "metamaterial transmission-line based antennas: design, challenges, and applications"," *IEEE Access*, vol. 8, pp. 144778–144808, 2020.

[32] M. Alibakhshikenari, F. Babaeian, B. S. Virdee et al., "A comprehensive survey on "various decoupling mechanisms with focus on metamaterial and metasurface principles applicable to SAR and MIMO antenna systems"," *IEEE Access*, vol. 8, pp. 192965–193004, 2020.

[33] M. Alibakhshikenari, "A new study to suppress mutual-coupling between waveguide slot array antennas based on metasurface bulkhead for MIMO systems," in *Proceedings of the 2018 Asia-Pacific Microwave Conference (APMC)*, pp. 500–502, Kyoto, Japan, November 2018.

[34] H. Li, J. Xiong, and S. He, "A compact planar MIMO antenna system of four elements with similar radiation characteristics and isolation structure," *IEEE Antennas and Wireless Propagation Letters*, vol. 8, pp. 1107–1110, 2009.

[35] Y. Yang, Q. Chu, and C. Mao, "Multiband MIMO antenna for GSM, DCS, and LTE indoor applications," *IEEE Antennas and Wireless Propagation Letters*, vol. 15, pp. 1573–1576, 2016.

[36] L. Kang, H. Li, X. Wang, and X. Shi, "Compact offset microstrip-fed MIMO antenna for band-notched UWB applications," *IEEE Antennas and Wireless Propagation Letters*, vol. 14, pp. 1754–1757, 2015.

[37] J. Y. Deng, L. X. Guo, and X. L. Liu, "An ultrawideband MIMO antenna with a high isolation," *IEEE Antennas and Wireless Propagation Letters*, vol. 15, pp. 182–185, 2016.

[38] J. Ren, W. Hu, Y. Yin, and R. Fan, "Compact printed MIMO antenna for UWB applications," *IEEE Antennas and Wireless Propagation Letters*, vol. 13, pp. 1517–1520, 2014.

[39] J. Deng, J. Li, L. Zhao, and L. Guo, "A dual-band inverted-F MIMO antenna with enhanced isolation for WLAN applications," *IEEE Antennas and Wireless Propagation Letters*, vol. 16, pp. 2270–2273, 2017.

[40] Alibakhshikenari, V. Mohammad, B. Singh et al., "Array antenna for synthetic aperture radar operating in X and Ku-Bands: a study to enhance isolation between radiation elements," in *Proceedings of the 12th European Conference on Synthetic Aperture Radar*, Aachen, Germany, June 2018.

[41] H. Arun, A. K. Sarma, M. Kanagasabai, S. Velan, C. Raviteja, and M. G. N. Alsath, "Deployment of modified serpentine structure for mutual coupling reduction in MIMO antennas," *IEEE Antennas and Wireless Propagation Letters*, vol. 13, pp. 277–280, 2014.

[42] N. Hussain and N. Kim, "Integrated microwave and mm-wave MIMO antenna module with 360 pattern diversity for 5G internet-of-things," *IEEE Internet of Things Journal*, p. 1, 2022.

[43] H. Huang, X. Li, and Y. Liu, "A low-profile, dual-polarized patch antenna for 5G MIMO application," *IEEE Transactions on Antennas and Propagation*, vol. 67, no. 2, pp. 1275–1279, 2019.

[44] D. Q. Liu, H. J. Luo, M. Zhang, H. L. Wen, B. Wang, and J. Wang, "An extremely low-profile wideband MIMO antenna for 5G smartphones," *IEEE Transactions on Antennas and Propagation*, vol. 67, no. 9, pp. 5772–5780, 2019.